eprints@whiterose.ac.uk
https://eprints.whiterose.ac.uk/

Adsorption of Aldehyde-Functional Diblock Copolymer Spheres onto Surface-Grafted Polymer Brushes via Dynamic Covalent Chemistry Enables Friction Modification

Edwin C. Johnson,* Spyridon Varlas,* Oleta Norvilaite, Thomas J. Neal, Emma E. Brotherton, George Sanderson, Graham J. Leggett, and Steven P. Armes*

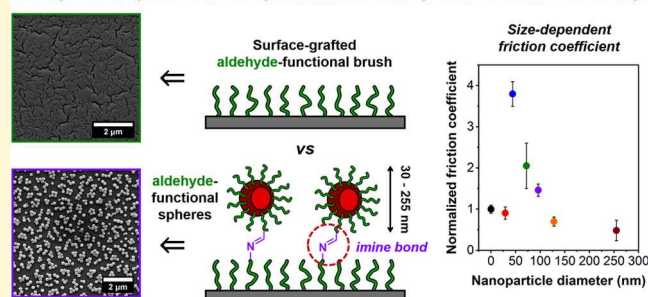Cite This: *Chem. Mater.* 2023, 35, 6109–6122

Read Online

ACCESS | Metrics & More | Article Recommendations | SI Supporting Information

ABSTRACT: Dynamic covalent chemistry has been exploited to prepare numerous examples of adaptable polymeric materials that exhibit unique properties. Herein, the chemical adsorption of aldehyde-functional diblock copolymer spherical nanoparticles onto amine-functionalized surface-grafted polymer brushes via dynamic Schiff base chemistry is demonstrated. Initially, a series of *cis*-diol-functional sterically-stabilized spheres of 30−250 nm diameter were prepared via reversible addition−fragmentation chain transfer (RAFT) aqueous dispersion polymerization. The pendent *cis*-diol groups within the steric stabilizer chains of these precursor nanoparticles were then oxidized using sodium periodate to produce the corresponding aldehyde-functional spheres.

Adsorption of Spheres onto Polymer Brushes via Dynamic Covalent Chemistry

Similarly, hydrophilic *cis*-diol-functionalized methacrylic brushes grafted from a planar silicon surface using activators regenerated by electron transfer atom transfer radical polymerization (ARGET ATRP) were selectively oxidized to generate the corresponding aldehyde-functional brushes. Ellipsometry and X-ray photoelectron spectroscopy were used to confirm brush oxidation, while scanning electron microscopy studies demonstrated that the nanoparticles did not adsorb onto a *cis*-diol-functional precursor brush. Subsequently, the aldehyde-functional brushes were treated with excess small-molecule diamine, and the resulting imine linkages were converted into secondary amine bonds via reductive amination. The resulting primary amine-functionalized brushes formed multiple dynamic imine bonds with the aldehyde-functional diblock copolymer spheres, leading to a mean surface coverage of approximately 0.33 on the upper brush layer surface, regardless of the nanoparticle size. Friction force microscopy studies of the resulting nanoparticle-decorated brushes enabled calculation of friction coefficients, which were compared to that measured for the bare aldehyde-functional brush. Friction coefficients were reasonably consistent across all surfaces except when particle size was comparable to the size of the probe tip. In this case, differences were ascribed to an increase in contact area between the tip and the brush-nanoparticle layer. This new model system enhances our understanding of nanoparticle adsorption onto hydrophilic brush layers.

INTRODUCTION

Dynamic covalent chemistry (DCC) involves the formation of dynamic covalent bonds (DCBs) under equilibrium conditions.[1−5] DCC can be used to design complex multicomponent materials or to generate combinatorial libraries.[3] Thus far, it has been successfully exploited for (bio)synthetic templating,[3,6−8] mechanochemistry,[9,10] construction of metal−organic frameworks,[11] as well as polymeric and colloidal materials engineering.[5]

In the context of polymer science, DCC has enabled the development of self-healing polymers and mechanically/macroscopically-responsive materials with adaptable properties.[12−17] It has also been utilized to design stimulus-responsive polymers, either through modification of their characteristics or by responding directly to the formation of DCBs, such as imine bonds,[18,19] acylhydrazone bonds,[20] Diels−Alder chem-

istry,[21] Se−N bonds,[22] boronic acid/*cis*-diol binding,[23−27] etc. Of particular relevance to the present study are imine bonds, which are formed when reacting an aldehyde with a primary amine. Such Schiff base chemistry has been used to generate covalent adaptable networks (CANs)[28,29] and hydrogels[5] for potential biomedical applications,[30] while it has also been exploited for conjugation of oligonucleotides to aldehyde-functional polymer brushes, which were prepared via partial
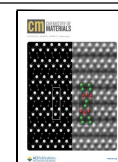
oxidation of a poly(2-hydroxyethyl methacrylate) (PHEMA) precursor brush.[31]

Recently, we reported a new hydrophilic aldehyde-functional polymer (PAGEO5MA).[32−34] This polymer can either be directly synthesized from the corresponding methacrylic monomer (AGEO5MA) or it can be generated via selective oxidation of a *cis*-diol-functional PGEO5MA precursor using sodium periodate (NaIO$_4$).[32] PAGEO5MA-based diblock copolymer spheres or vesicles can be reacted with various amino acids (e.g., glycine or L-histidine) via Schiff base chemistry followed by reductive amination.[33,35] PAGEO5MA-based diblock copolymer worms form soft, free-standing gels that exhibit strong mucoadhesion,[34] while PAGEO5MA brushes grafted from a planar surface can be reacted with model globular proteins, such as bovine serum albumin (BSA).[36] This involves the formation of multiple imine bonds between the aldehyde groups on the brush chains and the primary amine groups located at the surface of the protein. Each individual imine bond is relatively weak and prone to hydrolysis, but a sufficient number of these bonds remain intact at any given time to ensure that the protein remains conjugated to the polymer brush.

The design of well-defined nanoparticle-brush hybrid surfaces enables the construction of complex interfacial structures and multicomponent materials with tailored properties. This offers potential applications ranging from energy storage and plasmonics to drug release and friction modification.[37−39] For example, Huck and co-workers examined the adsorption of gold nanoparticles within or onto polymer brushes.[39−42] In this case, nanoparticle adsorption occurred via non-covalent electrostatic interactions, rather than by DCC.

Herein, we report the adsorption of aldehyde-functional diblock copolymer spherical nanoparticles of varying size onto amine-functionalized surface-grafted polymer brushes via DCC to generate a library of nanoparticle-brush planar surfaces with tunable friction coefficients. More specifically, a PGEO5MA$_{34}$ precursor was chain-extended with 2-hydroxypropyl methacrylate (HPMA) to generate a series of kinetically-trapped diblock copolymer spheres via reversible addition−fragmentation chain transfer (RAFT) aqueous dispersion polymerization (Scheme 1). These PGEO5MA$_{34}$-PHPMA$_y$ (denoted GO$_{34}$-H$_y$) diblock copolymer nanoparticles were analyzed by dynamic light scattering (DLS), small-angle X-ray scattering (SAXS), and electron microscopy. Their pendent *cis*-diol groups were then selectively oxidized using a stoichiometric amount of NaIO$_4$ under mild conditions with no loss of colloidal stability. The resulting aldehyde-functional PAGEO5MA$_{34}$-PHPMA$_y$ (denoted AGO$_{34}$-H$_y$) nanoparticles were then exposed to a series of hydrophilic PAGEO5MA brushes, which had been previously reacted with a small-molecule diamine. Dynamic imine bond formation between the nanoparticles and the primary amine-functional brushes led to their chemical adsorption. Subsequently, friction force microscopy was used to examine the relationship between nanoparticle diameter, surface topography, and measured friction coefficient.

■ RESULTS AND DISCUSSION

A PGEO5MA$_{34}$ (or GO$_{34}$) precursor was first synthesized via RAFT solution polymerization of GEO5MA in ethanol at 70 °C using a non-ionic trithiocarbonate chain transfer agent, following a similar experimental protocol to that previously reported by our group (Scheme S2).[32,33] A final GEO5MA

Scheme 1. Schematic Illustration of the Synthesis of *cis*-Diol-Functional GO$_{34}$-H$_y$ Diblock Copolymer Spheres (where y = 125−1500) via RAFT Aqueous Dispersion Polymerization of HPMA at 10% w/w Solids Using a GO$_{34}$ Precursor, and Their Subsequent Selective Oxidation Using NaIO$_4$ for the Preparation of Aldehyde-Functional AGO$_{34}$-H$_y$ Diblock Copolymer Spheres at 10% w/w Solids
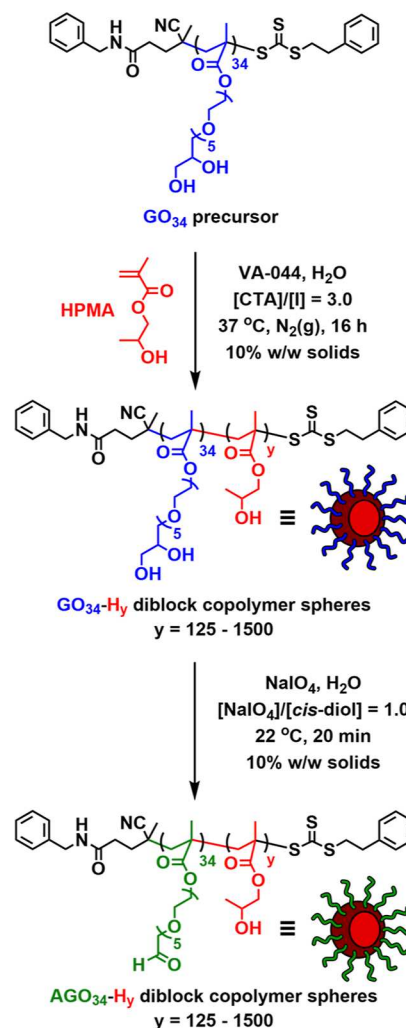
conversion of 86% was achieved after 180 min, as determined by ^{1}H NMR analysis in CD$_3$OD. End-group analysis of the purified PGEO5MA homopolymer using the same technique indicated a mean degree of polymerization (DP) of 34 (Figure S1). Size exclusion chromatography (SEC) analysis (DMF eluent containing 10 mM LiBr) for this GO$_{34}$ precursor revealed a narrow molecular weight distribution with an apparent number-average molecular weight (M_n) of 15.8 kg mol^{-1} and a relatively low dispersity (M_w/M_n) of 1.16 (Figure S2). This latter parameter suggested a well-controlled RAFT polymerization.

Based on our recent experience,[33] we anticipated that this relatively massive *cis*-diol-functional GO$_{34}$ precursor should produce kinetically-trapped diblock copolymer spheres when conducting RAFT aqueous dispersion polymerization syntheses at a sufficiently low copolymer concentration (e.g., 10% w/w solids). Accordingly, this water-soluble GO$_{34}$ precursor was subsequently chain-extended via RAFT aqueous dispersion polymerization of HPMA (H) at 37 °C to afford a series of
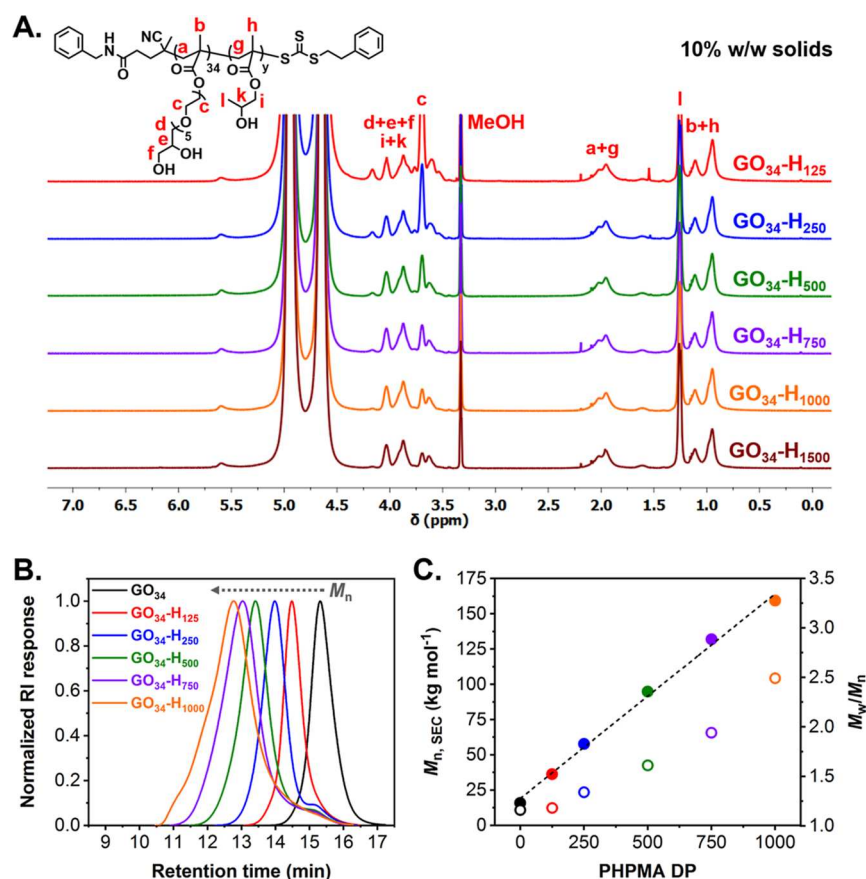
Figure 1. (A) Stacked ^1H NMR spectra (CD$_3$OD) recorded for a series of molecularly-dissolved GO$_{34}$-H$_y$ diblock copolymers (where $y = 125-1500$) prepared via RAFT aqueous dispersion polymerization of HPMA at 10% w/w solids. (B) Normalized SEC traces (refractive index detector) recorded for the GO$_{34}$ precursor (black line), and a series of GO$_{34}$-H$_y$ diblock copolymers (where $y = 125$, red line; $y = 250$, blue line; $y = 500$, green line; $y = 750$, purple line; and $y = 1000$, orange line) prepared at 10% w/w solids (DMF + 10 mM LiBr eluent). (C) Evolution of M_n (filled circles) and M_w/M_n (empty circles) as a function of target PHPMA DP for a series of GO$_{34}$-H$_y$ diblock copolymers prepared at 10% w/w solids, as determined by SEC RI analysis using a series of PMMA calibration standards.

GO$_{34}$-H$_y$ diblock copolymer spheres at 10% w/w solids (Scheme 1). The target PHPMA DP (y) was systematically varied from 125 to 1500 to produce nanoparticles of increasing size. Near-quantitative HPMA conversions (>99%) were achieved within 16 h in all cases, as determined by ^1H NMR studies in CD$_3$OD (Figure 1A and Table S1). SEC analysis confirmed that the GO$_{34}$ precursor was efficiently chain-extended, with M_n values for the resulting GO$_{34}$-H$_y$ diblock copolymers increasing linearly when targeting higher PHPMA DPs. Relatively low dispersities ($M_w/M_n \leq 1.34$) were calculated for the GO$_{34}$-H$_{125}$ and GO$_{34}$-H$_{250}$ diblock copolymers, but significantly higher values were obtained when targeting longer PHPMA blocks (Figure 1B,C and Table S1). These observations are broadly consistent with previously reported data when targeting high core-forming block DPs using aqueous PISA protocols.[43] A weak high-molecular-weight shoulder was only observed for GO$_{34}$-H$_{1000}$: this feature can be attributed to chain transfer to polymer or termination by recombination owing to traces of dimethacrylate impurities within the HPMA monomer.[44,45] Unfortunately, the GO$_{34}$-H$_{1500}$ diblock copolymer proved to be poorly soluble in DMF and hence was unsuitable for SEC analysis.

Next, the size and morphology of the GO$_{34}$-H$_y$ diblock copolymer nanoparticles was assessed using a series of scattering and microscopy techniques. In particular, DLS analysis confirmed narrow, monomodal particle size distribu-

tions. Targeting higher PHPMA DPs resulted in a monotonic increase in the mean hydrodynamic diameters (D_h) from 30 to 250 nm with relatively low polydispersities (PD $\leq$ 0.08) (Figure 2A,B and Table S1). Subsequently, SAXS analysis verified these DLS data. Zero gradients were observed in the low-q region (where q is the scattering vector) of $I(q)$ vs q plots, which suggested a spherical morphology in each case. Furthermore, a progressive shift in the local minimum at lower q was evident when targeting higher PHPMA DPs, while a satisfactory fit was obtained for each SAXS pattern using a well-documented spherical micelle model (Figure 2C).[46] This enabled calculation of the overall volume-average particle diameters (D_{SAXS}) for this nanoparticle series, which were consistent with the corresponding DLS data (Figure S4 and Table S1).

Morphologies for the entire series of *cis*-diol-functional GO$_{34}$-H$_y$ diblock copolymer nanoparticles were examined by conventional transmission electron microscopy (TEM). Well-defined, uniform spherical nanoparticles were observed in all cases (Figure 2D). Corresponding particle size distribution histograms were constructed via digital image analysis that enabled estimation of the number-average sphere diameters (D_{TEM}) (Figure S3). As expected for particle size distributions of finite width, D_{TEM} values were moderately lower than D_{SAXS}, whereas the z-average diameters (D_h) determined by DLS were always systematically higher (Figure S4 and Table S1).
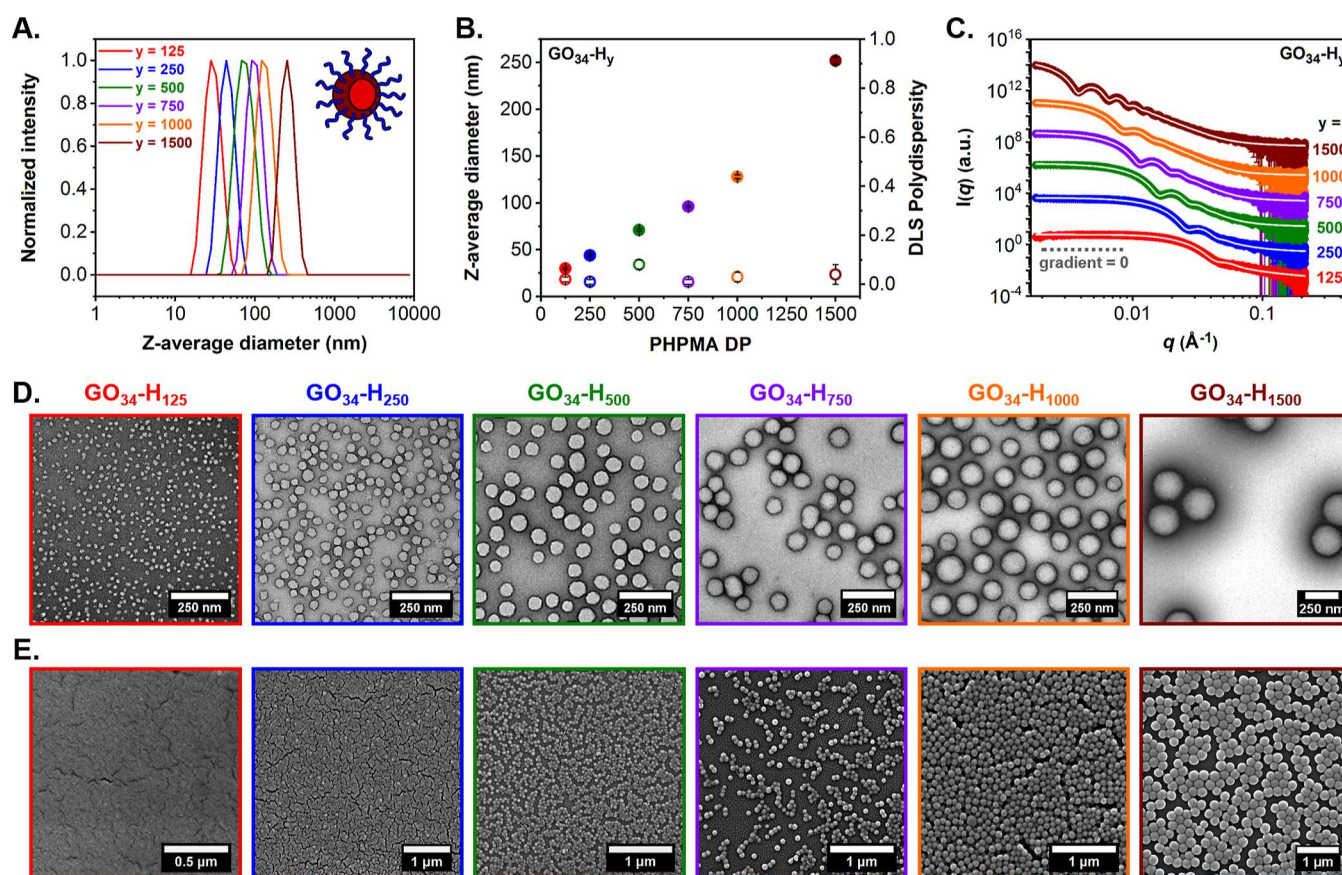
Figure 2. Summary of characterization data obtained for a series of *cis*-diol-functional GO_{34}-H_y diblock copolymer spheres (where $y = 125-1500$) prepared via RAFT aqueous dispersion polymerization of HPMA at 10% w/w solids: (A) intensity-weighted DLS particle size distributions, (B) evolution of *z*-average diameter (filled circles) and corresponding DLS polydispersity (PD) (empty circles) with increasing target PHPMA DP, (C) SAXS patterns recorded for 1.0% w/w aqueous copolymer dispersions and corresponding data fits (white solid lines) applied to each SAXS pattern using a well-known spherical micelle model,[46] (D) representative TEM images obtained using a uranyl formate stain, and (E) representative SEM images.

Scanning electron microscopy (SEM) and atomic force microscopy (AFM) were also utilized for imaging of the dried aqueous dispersions of GO_{34}-H_y diblock copolymer spheres. These complimentary techniques provided further evidence for well-defined spherical nanoparticle morphologies when examining significantly larger numbers of particles than TEM (Figures 2E and S5).

Moreover, aqueous electrophoresis studies were performed for all copolymer dispersions in a background salt concentration of 1 mM KCl at pH 6.8 (i.e., the solution pH of the deionized water used for nanoparticle syntheses, their chemical modification, and subsequent analyses) with zeta potentials ranging between −13 and −17 mV, regardless of the PHPMA DP (Figure S6 and Table S1).

To further evaluate the extent of polymerization control achieved for such PISA syntheses and to monitor the evolution in particle size and polydispersity, kinetic studies were conducted during the synthesis of GO_{34}-H_{1000} diblock copolymer spheres at 37 °C when targeting 10% w/w solids. More specifically, aliquots were periodically withdrawn from the polymerizing mixture (every 30 min for the first 6 h and again after 8 h) and immediately quenched upon exposure to air, while cooling to 20 °C. These samples were then analyzed by ^{1}H NMR spectroscopy in CD_3OD for HPMA conversion calculations, SEC for determination of M_n and M_w/M_n, DLS

for measurement of D_h and PD, as well as TEM for assessing the intermediate nanoparticle morphologies.

On inspection of the constructed conversion vs time curve, almost all of the HPMA monomer (99%) had reacted within 8 h. The corresponding semi-logarithmic plot revealed a pseudo-first-order kinetic profile for this aqueous dispersion polymerization that was separated in three distinct reaction regimes (Figure 3A and Table S2). During the first 90 min, relatively slow RAFT solution polymerization occurred to produce water-soluble GO_{34}-H_y diblock copolymer chains. After approximately 90 min—which corresponds to 10% monomer conversion, or a PHPMA DP of 100—a ∼3.5-fold increase in the rate of HPMA polymerization was observed, which indicated the onset of micellar nucleation. At this stage, the formed nascent micelles immediately become swollen with unreacted monomer, which leads to a relatively high local concentration and hence a much faster rate of polymerization.[45] Finally, an additional four-fold rate enhancement was observed after ∼180 min (42% HPMA conversion, PHPMA DP = 420). This phenomenon has been reported for similar PISA formulations and is tentatively attributed to the formation of more compact nanoparticles via gradual expulsion of residual solvent molecules from the nanoparticle cores.[47,48] Importantly, SEC analysis revealed a linear evolution in M_n with increasing monomer conversion, suggesting a controlled RAFT polymerization at each stage (Figure 3B and Table S2).
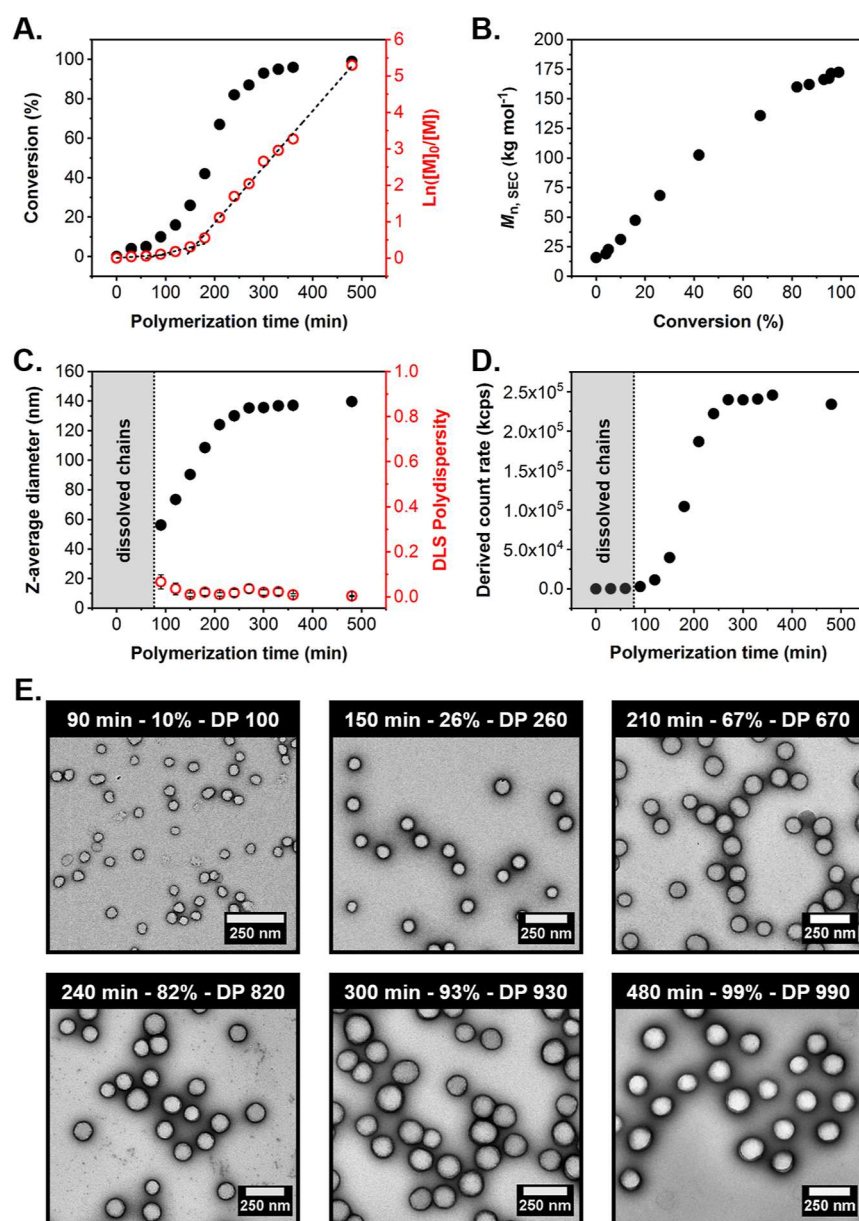
Figure 3. (A) HPMA conversion vs time curve (black filled circles) and corresponding $\ln([M]_0/[M])$ vs time plot (red empty circles), determined by ^{1}H NMR spectroscopy during the synthesis of GO$_{34}$-H$_{1000}$ diblock copolymer spheres via RAFT aqueous dispersion polymerization of HPMA at 37 °C when targeting 10% w/w solids. (B) Evolution of M_n with increasing HPMA conversion for a series of intermediate GO$_{34}$-H$_y$ diblock copolymers prepared at 10% w/w solids, as calculated from SEC analysis (refractive index detector) using a series of PMMA calibration standards (DMF + 10 mM LiBr eluent). (C) Evolution of z-average diameter (black filled circles) and corresponding DLS polydispersity (PD) (red empty circles) during the polymerization, and (D) derived count rate vs time plot (black filled circles) for the same aqueous PISA formulation. (E) Representative TEM images recorded for GO$_{34}$-H$_y$ diblock copolymer nanoparticles formed at intermediate HPMA conversions, obtained using a uranyl formate stain. The polymerization time, instantaneous HPMA conversion, and corresponding PHPMA DP are indicated in each case.

Further insights into the onset of micellar nucleation and size evolution were provided by DLS analysis of the same samples withdrawn at intermediate HPMA conversions from the reaction mixture. No particles were detected within the first 90 min, as judged by the relatively low scattering intensity (derived count rate <370 kcps), suggesting the initial formation of molecularly-dissolved copolymer chains (Figure 3C,D and Table S2). Once micellar nucleation occurred at 90 min (10% HPMA conversion), a linear increase in D_h was observed from 56 nm up to 124 nm over the following 120 min (67% HPMA conversion after 210 min), with a corresponding sequential increase in the derived count rate up to 186,700

kcps. As the remaining monomer within the nanoparticle cores is consumed, it is no longer replenished from the continuous phase. Additionally, as the growing nanoparticles become less swollen with the monomer, they also become denser (as low-density monomer is converted to higher-density polymer). Thus, only a rather modest increase in D_h and derived count rate was observed between this time point and the end of the polymerization. Notably, the D_h of 140 nm measured for the final GO$_{34}$-H$_{1000}$ diblock copolymer spheres produced during this kinetic study is comparable to that obtained for the respective sample with the same composition synthesized in the absence of any periodic sampling of the reaction mixture
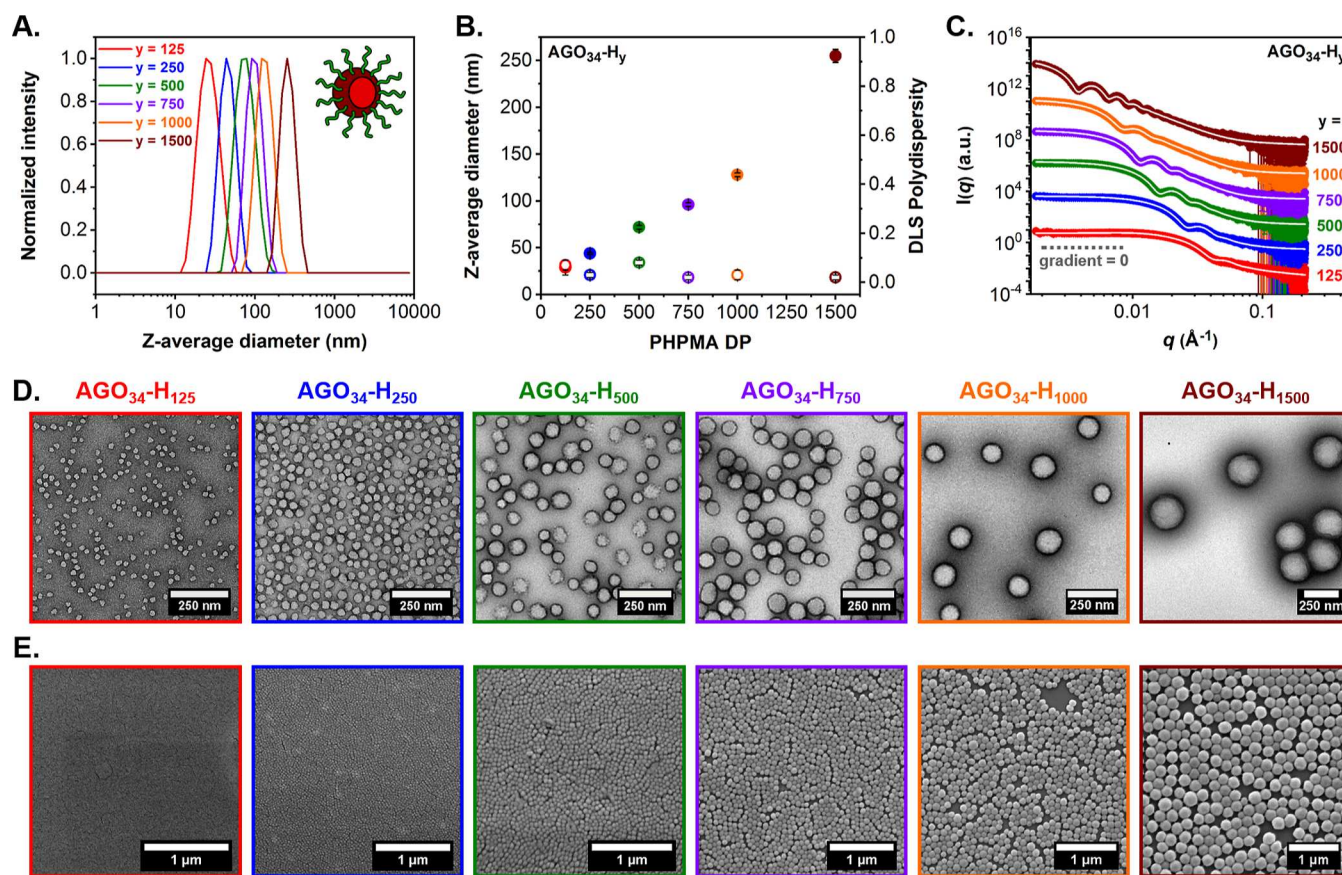
Figure 4. Summary of characterization data obtained for a series of aldehyde-functional AGO_{34}-H_y diblock copolymer spheres (where $y = 125-$
1500): (A) intensity-weighted DLS particle size distributions, (B) evolution of z-average diameter (filled circles) and corresponding DLS
polydispersity (PD) (empty circles) with increasing target PHPMA DP, (C) SAXS patterns recorded for 1.0% w/w aqueous copolymer dispersions
and corresponding data fits (white solid lines) applied to each SAXS pattern using a well-known spherical micelle model,[46] (D) representative TEM
images obtained using a uranyl formate stain, and (E) representative SEM images.

(D_h = 128 nm). However, the D_h values measured for the
series of GO_{34}-H_y diblock copolymer spheres isolated during
this kinetic study are significantly higher than those observed
when targeting compositionally similar diblock copolymers
(e.g., D_h = 90 nm for GO_{34}-H_{260} at 26% HPMA conversion vs
D_h = 44 nm for GO_{34}-H_{250} at >99% HPMA conversion)
(Tables S1 and S2). This discrepancy is attributed to the
monomer-swollen nature of the spheres in the former case.
Importantly, DLS PDs remained below 0.07 for all kinetic
samples, while TEM analysis confirmed the formation of near-
monodisperse spheres of increasing size at higher HPMA
conversions (Figures 3E and S7).

Recently, we reported that the pendent *cis*-diol functionality
on PGEO5MA homopolymers, PGEO5MA-based diblock
copolymer nano-objects, and PGEO5MA brushes can be
selectively oxidized using sodium periodate ($NaIO_4$) under
mild reaction conditions to form the respective aldehyde-
functional PAGEO5MA-based materials. The resulting PA-
GEO5MA chains can be further functionalized using various
primary amines (including amino acids) via reductive
amination.[32,33,35,36] In the present study, our aim was to
extend these reports by investigating whether dynamic imine
bond formation could be used to promote the chemical
adsorption of PAGEO5MA-stabilized diblock copolymer
spheres of varying size onto surface-grafted amine-function-
alized PDAGEO5MA brushes to produce a library of model

soft hybrid surfaces of tuneable topography for friction
coefficient measurements.

Accordingly, selective oxidation of the precursor GO_{34}-H_y
diblock copolymer spheres was achieved by addition of $NaIO_4$
to 10% w/w aqueous copolymer dispersions at 22 °C in the
dark for 20 min to yield a series of aldehyde-functional
PAGEO5MA$_{34}$-PHPMA$_y$ (AGO_{34}-H_y) spheres, where y = 125-
1500 (Scheme 1). A [*cis*-diol]/[$NaIO_4$] molar ratio of unity
was employed to ensure 100% oxidation of the PGEO5MA
repeat units, as previously reported by Brotherton et al.[33]
Oxidized nanoparticles were subsequently diluted to 1% w/w
solids prior to dialysis against deionized water to remove spent
oxidant and the formaldehyde byproduct. ^1H NMR spectros-
copy analysis (CD_3OD) confirmed the appearance of a new
signal at approximately 3.5 ppm, whose intensity was
proportional to the *cis*-diol content of each copolymer. This
new feature is attributed to the formation of aldehyde groups
in their hydrated germinal diol form, indicating the successful
oxidation of the steric stabilizer chains (Figure S8).[32] In
principle, the secondary alcohol groups within the hydrophobic
PHPMA block could be oxidized to form ketone groups.
However, $NaIO_4$ is highly selective toward *cis*-diol groups,[32,49]
so in practice this side reaction was not observed under the
stated conditions.

Additionally, SEC analysis of the resulting AGO_{34}-H_y
diblock copolymers (DMF + 10 mM LiBr eluent) indicated
a discernible increase in M_n and M_w/M_n compared to the

Scheme 2. Schematic Illustration of the Grafting of PGEO5MA Homopolymer Brushes from Planar Silicon Wafers via SI-ARGET ATRP, Their Selective Oxidation to Produce Aldehyde-Functional PAGEO5MA Brushes, Their Subsequent Functionalization with a Hydrophilic Diamine (Jeffamine EDR-148) to Generate PDAGEO5MA Brushes, Followed by Chemical Adsorption of a Series of AGO$_{34}$-H$_y$ Diblock Copolymer Spheres (where y = 125−1500) onto Such PDAGEO5MA Brushes to Produce a Library of Nanoparticle-Decorated AGO$_{34}$-H$_y$@PDAGEO5MA Surfaces via DCC
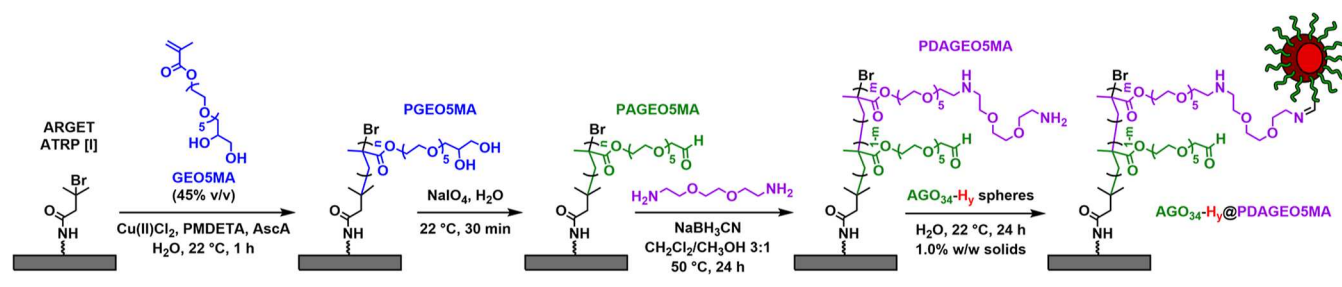
original GO$_{34}$-H$_y$ copolymers. Moreover, the development of high-molecular-weight shoulders led to significantly broader molecular-weight distributions, with such features being more pronounced for shorter PHPMA DPs (i.e., when the corona-forming PAGEO5MA block makes a larger contribution to the overall diblock copolymer molecular-weight distribution) (Figure S9 and Table S3). These observations are attributed to aldol cross-linking reactions occurring between the aldehyde and *cis*-diol groups of the stabilizer block chains at intermediate conversions during periodate oxidation or between the pendent aldehyde groups of PAGEO5MA and the hydroxyl groups of the partially hydrated PHPMA block.[33]

Importantly, DLS and SAXS analyses confirmed that periodate oxidation did not affect the particle size or colloidal stability of the developed AGO$_{34}$-H$_y$ diblock copolymer spheres. These nanoparticles exhibit almost identical D_h and D_{SAXS} diameters to those determined for the precursor GO$_{34}$-H$_y$ spheres prior to oxidation (Figures 4A−C and S11 and Table S3). These data were further supported by TEM, SEM, and AFM images, which indicated that near-monodisperse spherical nanoparticles of tuneable size were obtained for the whole diblock copolymer series (Figures 4D,E and S10−S12 and Table S3). Furthermore, no significant changes in zeta potential were observed by aqueous electrophoresis studies for the periodate-treated spheres (values ranged between −15 and −19.5 mV) (Figure S13 and Table S3).

So far we have demonstrated the synthesis of near-monodisperse kinetically-trapped AGO$_{34}$-H$_y$ spheres of increasing size. As highlighted above, our aim was to generate suitably modified PDAGEO5MA brushes to enable the chemical adsorption of such nanoparticles via dynamic imine bond formation. The synthetic route employed for the preparation of nanoparticle-decorated AGO$_{34}$-H$_y$@PDA-GEO5MA hybrid surfaces is illustrated in Scheme 2.

Initially, ATRP initiator groups were introduced onto planar silicon wafers using a previously reported experimental protocol.[50] Surface-initiated activators regenerated by electron transfer atom transfer radical polymerization (SI-ARGET ATRP) was then used to graft uniform PGEO5MA brushes of ~120 nm dry thickness, as determined via ellipsometry (Table S4), from these modified substrates, following a procedure recently reported by our group.[36] While, ultimately, aldehyde functionality is required for diamine functionalization and subsequent nanoparticle adsorption, *cis*-diol-functional PGEO5MA brushes were first grown herein as they allow for preparation of more densely grafted surfaces compared to

brushes synthesized directly from polymerization of the respective AGEO5MA monomer.[36]

To produce the analogous aldehyde-functional PAGEO5MA brushes, such PGEO5MA brushes were exposed to an aqueous NaIO$_4$ solution for 30 min at 22 °C (Scheme 2).[36] Selective oxidation of the pendent *cis*-diol groups was confirmed by both ellipsometry and X-ray photoelectron spectroscopy (XPS) studies. Periodate oxidation should lead to a reduction in the molecular weight of each repeat unit owing to the loss of a formaldehyde molecule.[32] Thus, given that the dry brush thickness is proportional to the polymer molecular weight,[51] complete oxidation of the PGEO5MA repeat units is expected to produce an approximate 8.5% reduction in dry thickness.[36] Indeed, ellipsometry measurements confirmed such a reduction in dry brush thickness equal to this theoretically expected value after exposing each PGEO5MA brush to NaIO$_4$ (mean dry PAGEO5MA brush thickness = 111 nm) (Table S4). Moreover, comparing the C 1s XPS data obtained for the PGEO5MA and PAGEO5MA brushes revealed a shift in the ratio of the O−$\underline{C}$=O, $\underline{C}$=O, $\underline{C}$−O−C/$\underline{C}$−O−H, and $\underline{C}$−H peaks that is consistent with brush oxidation (Figure S14).[36]

Recently, we have reported that PAGEO5MA-based chains,[32] diblock copolymer nano-objects,[33,35] and brushes[36] can be further functionalized with various amino acids, such as L-histidine, via reductive amination. For surface-grafted PAGEO5MA brushes, this involves immersion into an aqueous solution containing the desired amine reagent and sodium cyanoborohydride (NaBH$_3$CN), prior to heating to 50 °C for 24 h. Herein, this protocol was adapted to functionalize PAGEO5MA brushes using a hydrophilic diamine (Jeffamine EDR-148) to prepare the corresponding PDAGEO5MA brushes, as illustrated in Scheme 2. In principle, this diamine reagent could react with two aldehyde groups, leading to either intramolecular or intermolecular cross-linking. In practice, this potential issue was minimized herein by using a large excess of diamine.[52] Furthermore, this derivatization reaction of the PAGEO5MA brushes with the diamine was performed in a binary solvent mixture (CH$_2$Cl$_2$/methanol 3:1), that is a poor solvent for the PAGEO5MA chains. Thus, the brushes were functionalized in their collapsed (rather than extended) conformation. This should limit diamine reaction with only the near-surface aldehyde groups of the brushes.[52−54]

The formation of diamine-functional PDAGEO5MA brushes was verified by XPS (Figure 5A) and quantified by ellipsometry (Table S4). For the latter technique, the measured increase in dry brush thickness is compared to the maximum increase calculated for complete diamine conjuga-
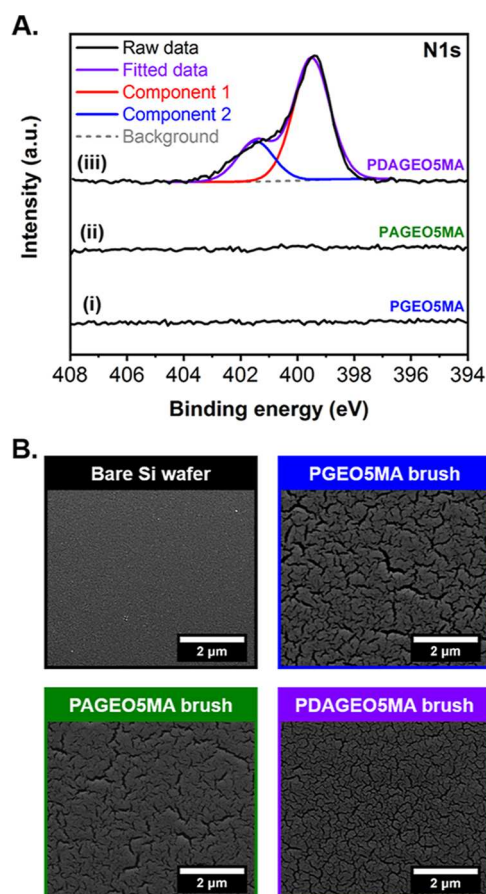
Figure 5. (A) High-resolution N 1s XPS data for surface-grafted (i) PGEO5MA (mean dry brush thickness = 121 nm), (ii) PAGEO5MA (mean dry brush thickness = 111 nm), and (iii) PDAGEO5MA (mean dry brush thickness = 129 nm) brushes (black lines). For the latter brush, the fitted data (purple line), individual components (red and blue lines), and subtracted background (gray dashed line) are also shown. (B) Representative SEM images recorded (after gold sputter coating) for a bare silicon wafer (black outline) and the surface-grafted PGEO5MA (blue outline), PAGEO5MA (green outline), and PDAGEO5MA (purple outline) dry brushes.

tion (assuming no cross-linking side-reactions). More specifically, the molecular weight of the brush repeat units should increase from 351 g mol^{-1} for PAGEO5MA to 483 g mol^{-1} for PDAGEO5MA, which would result in a theoretical 38% increase in dry brush thickness. Hence, the mean degree of diamine functionalization throughout the entire PDAGEO5-MA brush layer was calculated to be 36 ± 4% for the entire brush series (Table S4).[55]

XPS analysis was also employed to examine the surface composition of PDAGEO5MA brushes. The high-resolution N1s spectra for PGEO5MA, PAGEO5MA, and PDAGEO5MA brushes are shown in Figure 5A. As expected, the PGEO5MA and PAGEO5MA brushes exhibited no N 1s signal. However, a prominent N 1s signal was observed for the PDAGEO5MA brush, indicating successful diamine conjugation to the PAGEO5MA brush via reductive amination. The two distinct component peaks observed in the modeled XPS data correspond to N$^+$ (blue line, 401.4 eV) and N^0 (red line, 399.5 eV, indicating the presence of neutral and protonated amines.[54,56] Each PDAGEO5MA brush was thoroughly rinsed with deionized water (pH 7) prior to drying for XPS analysis. The pK_a of the protonated primary amine of a similar Jeffamine

molecule shifts from 9.7 in solution to 7.1 when grafted to a surface.[57] A similar pK_a shift is observed for poly(tertiary amine methacrylate)-based brushes, whereby the pK_a of surface-grafted chains is significantly lower than that of either free chains or the corresponding monomer.[50,58−61] Peak area analysis revealed a N^0/N$^+$ atomic ratio of approximately 3.0. Notably, this relatively low degree of amine protonation (25%) suggests a similar pK_a shift for the amine groups within the PDAGEO5MA brushes.

The degree of diamine functionalization was also examined by calculating the corresponding N/O atomic ratio. However, XPS only interrogates the upper ∼10 nm of the dry brush,[62] so such data only provide the near-surface compositions, rather than throughout the whole brush layer. By comparing the experimental N/O atomic ratio to its maximum theoretical value (corresponding to 100% functionalization), the degree of functionalization was determined to be 56% for the upper surface of the PDAGEO5MA brush. This is significantly higher than the mean degree of functionalization calculated from ellipsometry measurements (36 ± 4%). This discrepancy provided evidence for the (partial) surface confinement of the diamine groups. This is not unexpected given that reductive amination was conducted in a poor solvent for the PAGEO5MA brush chains.[52−54]

SEM images acquired for a bare silicon wafer and representative examples of the surface-grafted PGEO5MA, PAGEO5MA, and PDAGEO5MA brushes are shown in Figure 5B. Clearly, a distinct change in the surface morphology was observed following the PGEO5MA brush grafting. The surface of each brush is relatively uniform, which is consistent with the corresponding ellipsometry data. However, multiple cracks were also observed for each polymer film. Since these features were not observed in the corresponding AFM images (Figure S15), they appear to be a drying artifact resulting either from the ultrahigh vacuum environment or the gold sputter coating required for SEM imaging.

Recently, we demonstrated the chemical adsorption of BSA onto a surface-grafted PAGEO5MA brush through the formation of multiple imine bonds between amines on the protein and the aldehyde groups on the polymer brush.[36] Herein, we used a complimentary approach to adsorb a series of aldehyde-functional AGO$_{34}$-H$_y$ diblock copolymer spheres of varying size onto amine-functionalized PDAGEO5MA brushes via the same DCC.

Nanoparticle adsorption onto PDAGE5OMA brushes was achieved via overnight immersion of the modified silicon wafers into 1% w/w aqueous diblock copolymer dispersions at 22 °C (Scheme 2). Representative SEM and AFM images of a series of the resulting AGO$_{34}$-H$_y$@PDAGEO5MA hybrid surfaces are shown in Figure 6A,B, respectively. Clearly, this facile dip-coating protocol led to efficient nanoparticle adsorption to the PDAGEO5MA brushes. The four largest AGO$_{34}$-H$_y$ diblock copolymer nanoparticle formulations (y = 500, 750, 1000, and 1500) could be distinctly observed via SEM, whereas the surface of the corresponding precursor PDAGEO5MA brush was essentially featureless (Figure 5B). Unfortunately, adsorption of the two smallest nanoparticle formulations (y = 125 and 250) could not be clearly visualized by SEM owing to insufficient resolution. However, AFM analysis confirmed the presence of all six types of nanoparticles at the brush surface (Figure 6B). Importantly, an AFM image of a bare dry PAGEO5MA brush indicated a relatively uniform topography with minimal surface roughness (Figure S15). In
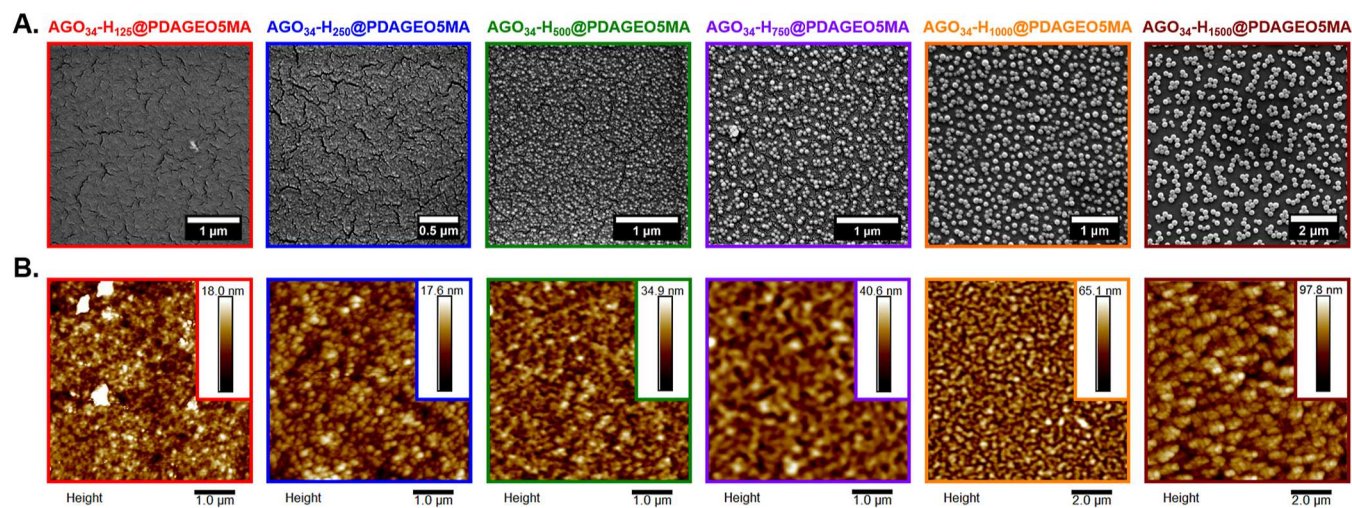
Figure 6. Representative (A) SEM and (B) AFM images (tapping mode) recorded for a series of nanoparticle-decorated AGO$_{34}$-H$_y$@PDAGEO5MA dry brushes (where y = 125, red outlines; y = 250, blue outlines; y = 500, green outlines; y = 750, purple outlines; and y = 1000, orange outlines; and y = 1500, burgundy outlines). The mean AGO$_{34}$-H$_y$ nanoparticle hydrodynamic diameter (D_h), as determined by DLS analysis, was 29 nm for y = 125, 44 nm for y = 250, 72 nm for y = 500, 96 nm for y = 750, 128 nm for y = 100, and 255 nm for y = 1500. Mean dry brush thickness for the initial PDAGEO5MA-based surfaces was 129 nm.

addition to visual confirmation of the adsorption of the AGO$_{34}$-H$_y$ diblock copolymer spheres, AFM height image analysis also revealed a significant increase in the roughness of each nanoparticle-decorated surface with increasing nanoparticle diameter.

The mean brush surface coverage by each nanoparticle sample was estimated by digital image analysis of the SEM images acquired for AGO$_{34}$-H$_y$@PDAGEO5MA surfaces coated with the four largest AGO$_{34}$-H$_y$ nanoparticles (y = 500−1500). This approach led to measurement of mean surface coverages of 31−38% (Figure S16). Such data are comparable to that reported in the literature for nanoparticle adsorption onto other polymer brushes[63−65] or bare substrates[35,66,67] via electrostatic interactions or covalent bond formation. Curiously, visual analysis of the AFM images acquired for the dried nanoparticle-coated surfaces indicated a notably higher degree of coverage. This discrepancy likely arises when further dehydration occurs on exposure of the samples to the ultrahigh vacuum during SEM imaging. This drying of the hybrid surfaces could result in particles separating on the surface, revealing the brush layer underneath. Given that XPS (Figures 5A and S14) indicated that 56% of the original aldehyde groups were converted into amines, such surface coverages suggest complete saturation of the available binding sites. Thus, despite the relatively weak nature of each individual imine bond (plus their propensity to undergo hydrolysis in aqueous solution), the DCC exploited herein leads to relatively efficient nanoparticle adsorption, presumably via formation of multiple imine bonds per nanoparticle. It is perhaps also worth mentioning that nanoparticle diffusion within a relatively dense brush layer is extremely unlikely, particularly for the larger nanoparticles.[68] As such, DCC is almost certain surface-confined.

To confirm that dynamic Schiff base chemistry is responsible for the observed nanoparticle adsorption (rather than merely non-specific binding), two control experiments were conducted. First, a bare silicon wafer was exposed to AGO$_{34}$-H$_{1000}$ spheres (AGO$_{34}$-H$_{1000}$@Si). Second, a *cis*-diol-functional PGEO5MA brush was exposed to GO$_{34}$-H$_{1000}$ spheres

(GO$_{34}$-H$_{1000}$@PGEO5MA) with SEM image analysis being used to quantify the extent of surface coverage in each case (Figure S17). Minimal nanoparticle adsorption onto the bare silicon wafer was observed (mean surface coverage ~1%), whereas no detectable nanoparticle adsorption was observed for the PGEO5MA brush, hence excluding physical adsorption as a means of nanoparticle conjugation.

The anti-fouling capabilities of the *cis*-diol functional PGEO5MA brushes toward both proteins[36] and sterically-stabilized nanoparticles (this work) highlight the importance of Schiff base chemistry in promoting nanoparticle adsorption. During their close approach to well-solvated polymer brush chains, such nanoparticles experience a repulsive force owing to the increase in osmotic pressure (as well as the concomitant reduction in entropic freedom).[69−72] The formation of DCBs between the spheres and each polymer brush is clearly essential for particles to overcome this repulsive barrier.

Importantly, the topography of hydrated nanoparticle-decorated AGO$_{34}$-H$_y$@PDAGEO5MA surfaces was examined by AFM (Figure S18). Both the PDAGEO5MA brush chains and the steric stabilizer PAGEO5MA chains expressed at the surface of the adsorbed nanoparticles should become swollen when exposed to water. Nevertheless, in accordance with the analysis performed in dry conditions, the attachment of the nanoparticles was evident when compared to the bare PAGEO5MA hydrated brush (Figure S15). Moreover, there is a significant apparent increase in nanoparticle surface coverage. The continued presence of the nanoparticles on the brush surface following a drying-hydration cycle further highlighted DCC as the driving force for their adsorption.

Clearly, DCC can be exploited for the immobilization of polymer nanoparticles to surface-grafted polymer brushes to generate a library of composite interfaces. In principle, this approach could be extended to attach other polymer nano-objects, including worms and vesicles, opening these hybrid interfaces to a range of applications such as nanoreactor capture to surfaces and programmable surface lubrication. For each of these applications, an understanding of the surface topography and its interaction with other materials is required.

In general, further development of this library of model nanoparticle-decorated brushes offers an opportunity to examine the role of topography on friction of soft surfaces, complementing existing alternative approaches.[73,74] By investigating the correlation between surface topography and lateral force exerted on a probe, we can elucidate apparent disparities in surface coverage depicted in AFM and SEM images. Additionally, this will facilitate understanding of the interaction between nanoparticle-brush surfaces and extrinsic systems.

The topography of each nanoparticle-brush hybrid surface was further examined by nanofriction measurements using friction force microscopy. The presence of the nanoparticles in the polymer film influences the lateral deflection of the AFM cantilever by modifying both the topography and the mechanical properties of the surface. Differences in specific interactions and adhesion are considered negligible since the steric stabilizer chains on the surface of the nanoparticles are chemically identical. Friction force microscopy studies were undertaken using the same AFM instrument. More specifically, each AGO_{34}-H_y@PDAGEO5MA brush was examined in aqueous solution at 24 °C. A single AFM tip (nominal radius of 10 nm) was used for all experiments, and the friction of each surface was normalized relative to a nanoparticle-free PAGEO5MA brush. Figure 7A shows the lateral photodetector response—which is proportional to the friction force—recorded for the AFM tip when increasing the normal load applied to each brush surface.
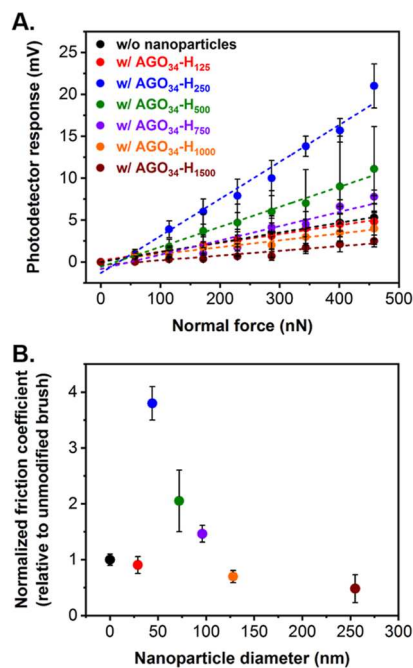
Friction force microscopy studies have been previously performed on polymer brushes.[75−77] According to these prior studies, the total frictional force (F_F) can be regarded as the sum of load-dependent (plowing) and area-dependent (shearing) terms.[78−80] The balance of these two components determines the relationship between applied load and friction. In the present work, a linear response to increasing load was observed for all surfaces. Consequently, each data set was analyzed using Amontons' law, $F_F = \mu F_N$, where F_N is the applied load and μ is the friction coefficient.[81] Hence, the gradient of the data fit is equal to the friction coefficient. As a single tip was used for all surfaces, normalization of these coefficients to the nanoparticle-free PAGEO5MA brush (black data in Figure 7A) was straightforward. These relative values are shown in Figure 7B as a function of the nanoparticle diameter (measured by DLS). Measurement of such relative friction coefficients is both common and highly reproducible.[82,83]

For the smallest AGO_{34}-H_{125} nanoparticles, the friction coefficient (μ) did not deviate significantly from that of the bare brush. However, a four-fold increase in this parameter was observed for the AGO_{34}-H_{250}@PDAGEO5MA brush. In this case, the nanoparticle radius (22 nm) is just over twice that of the nominal AFM tip radius (10 nm). However, as the nanoparticle radius increased further, a gradual reduction in the friction coefficient was observed with the AGO_{34}-$H_{1000/1500}$@PDAGEO5MA brushes exhibiting ∼50% of the bare PAGEO5MA brush friction coefficient.

These results are schematically presented in Scheme 3. For the nanoparticle-free PAGEO5MA-functionalized surface

Figure 7. (A) AFM photodetector response as a function of applied normal force for a hydrated PAGEO5MA brush (black data) and a series of nanoparticle-decorated AGO_{34}-H_y@PDAGEO5MA hydrated surfaces (where y = 125, red data; y = 250, blue data; y = 500, green data; y = 750, purple data; y = 1000, orange data; and y = 1500, burgundy data), obtained by friction force microscopy analysis. In each case, the gradient obtained from the linear fits to each data set was used to determine the corresponding friction coefficient. (B) Normalized friction coefficients calculated for a series of nanoparticle-decorated AGO_{34}-H_y@PDAGEO5MA surfaces relative to that of a PAGEO5MA brush as a function of nanoparticle diameter.

Scheme 3. Schematic Illustration of the Interaction of the AFM Tip with (A) a Bare PAGEO5MA-Functionalized Surface, (B) an AGO_{34}-H_{250}@PDAGEO5MA Surface Decorated with Nanoparticles of Comparable Size to the AFM Tip, and (C) an AGO_{34}-H_{1500}@PDAGEO5MA Surface Decorated with Nanoparticles Significantly Larger in Size than the AFM Tip. According to Figure 7B, a Significant Increase in Relative friction Coefficient is Observed for Scenario B
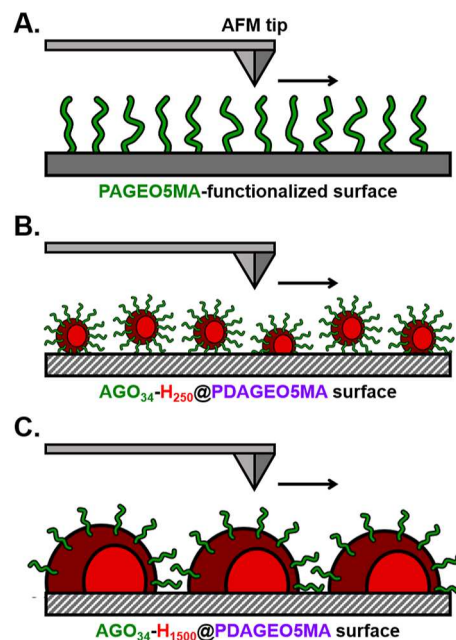
(Scheme 3A), the AFM probe tip simply shears over the surface, leading to a relatively low friction coefficient. For particles that are slightly larger than the AFM probe, a significant increase in the tip-sample contact area occurs at contact points between particles, leading to an increase in the rate of energy dissipation and hence in the friction force. However, as the particle size increases, the significance of these points of increased contact area decreases rapidly, and the friction coefficient reduces to a value slightly below that of the brush alone. The observed increase and subsequent decrease in the friction felt by the probe are thus ascribed to variations in contact surface area of the tip. Penetration of the tip into the interstices of particles increases the contact surface area, leading to additional adhesion and drag (Scheme 3B).[84] For significantly larger nanoparticles, their diameter is much larger than the tip dimensions, and their interfacial curvature approaches that of the planar surface (Scheme 3C). The reduction in relative friction for brushes decorated with the largest nanoparticles is tentatively attributed to differences in elastic moduli between the steric stabilizer chains and the brush chains. This is not surprising given their differences in free volume.[85−87] Given the complexity of these composite interfaces, a more nuanced modeling approach might reveal further details about the surfaces. In practice, Amonton's law is sufficient to account for the observed change in photodetector response. As such, we adopted Occam's razor and applied the simplest model to interpret the collected friction data.

Notably, surface forces apparatus is commonly employed to assess macroscopic surface friction.[88] For example, vulcanized rubber coated with poly(methyl methacrylate) particles (at similar surface coverages to those presented herein) exhibited a monotonic reduction in friction with increasing particle size.[88] Similarly, a significantly lower friction coefficient was observed within the boundary lubrication regime when conducting tribology experiments on epoxy-functionalized diblock copolymer nanoparticles covalently attached onto a planar stainless-steel substrate relative to comparable measurements performed using similar nanoparticles bearing no epoxy groups.[67] Nevertheless, we posit that friction force studies via AFM are ideally suited for probing subtle differences in surface roughness for the nanoparticle-decorated brush surfaces reported herein. In this context, an interesting finding was reported by Peña-Parás et al., who used wear measurements to assess friction for a series of particle lubricants.[89] This team found that using particles of intermediate size led to significantly less wear compared to both larger and smaller particles. This was attributed to the former particles being comparable in size to the surface roughness of the planar substrate. Thus, adsorption of such particles within the surface interstices reduced the overall surface roughness.

■ CONCLUSIONS

DCC has been exploited to promote chemical adsorption of a series of aldehyde-functional AGO_{34}-H_y diblock copolymer spheres (y = 125−1500) of varying size onto amine-functionalized polymer brushes. First, a series of cis-diol-functional precursor GO_{34}-H_y diblock copolymer nanoparticles were prepared via RAFT aqueous dispersion polymerization and characterized by DLS, SAXS, TEM, SEM, and AFM. Well-defined spheres of increasing size were obtained when targeting higher PHPMA DPs. Kinetic studies during the synthesis of GO_{34}-H_{1000} diblock copolymer spheres revealed a linear increase in M_n with HPMA conversion and a monotonic

increase in particle D_h with polymerization time. Subsequently, selective oxidation of GO_{34}-H_y nanoparticles using sodium periodate produced the corresponding aldehyde-functional AGO_{34}-H_y nanoparticles with no discernible changes in either particle size or colloidal stability. In parallel studies, PGEO5MA precursor brushes were grafted from planar silicon wafers using surface-initiated ARGET ATRP. Ellipsometry and XPS analyses were used to confirm $NaIO_4$ oxidation to afford the corresponding PAGEO5MA brushes and their subsequent chemical modification using a hydrophilic diamine in excess to generate amine-functionalized PDAGEO5MA brushes. This derivatization was deliberately performed in a poor solvent for the PAGEO5MA brush to ensure a surface-confined reaction. A control experiment confirmed that the precursor PGEO5MA brush was strongly resistant to nanoparticle adsorption. In contrast, the amine-functionalized PDAGEO5MA brushes readily formed imine bonds with the aldehyde-functional AGO_{34}-H_y spheres. Thus DCC can be used to promote chemical adsorption of such nanoparticles. SEM analysis of AGO_{34}-H_y@PDAGEO5MA surfaces indicated a mean surface coverage of 33 ± 4% for the whole nanoparticle series. Moreover, friction force microscopy studies of such nano-particle-decorated surfaces enabled calculation of friction coefficients, which were compared to that of a bare PAGEO5MA brush. Since the chemical structure of the steric stabilizer chains in the nanoparticles is the same regardless of their size, any observed variation in the friction coefficient can be attributed to changes in surface topography associated with nanoparticle adsorption. Reasonably consistent friction data were observed for all surfaces, except when the sphere diameter was comparable to the width of the AFM probe tip. In this case, the tip can penetrate between adjacent nanoparticles, which leads to a significant increase in contact area between the tip and the brush-nanoparticle layer and hence a higher friction coefficient. In principle, such systems provide useful model substrates for conducting friction force studies of soft surfaces. Moreover, the chemical adsorption of aldehyde-functional nanoparticles onto well-defined brushes via DCC is expected to be a generic approach. In particular, we are currently exploring the adsorption of enzyme-loaded diblock copolymer vesicles onto such brushes to produce surface-immobilized nanoreactors for enzyme-mediated catalysis applications.

■ EXPERIMENTAL SECTION

Materials, characterization techniques, and detailed synthesis protocols are provided in the Supporting Information.

■ ASSOCIATED CONTENT

ⓢ Supporting Information

The Supporting Information is available free of charge at https://pubs.acs.org/doi/10.1021/acs.chemmater.3c01227.

> Materials and characterization techniques, synthetic protocols, ^{1}H NMR spectrum and SEC curves for the GO_{34} precursor, characterization data for GO_{34}-H_y and AGO_{34}-H_y diblock copolymer spheres, additional TEM images obtained during kinetic studies for the synthesis of GO_{34}-H_{1000} diblock copolymer spheres, and characterization data for bare polymer brushes and for brushes modified with (A)GO_{34}-H_y diblock copolymer spheres (PDF)

■ AUTHOR INFORMATION

Corresponding Authors

Edwin C. Johnson − *Department of Chemistry, University of Sheffield, Sheffield S3 7HF, U.K.;* ⬤ orcid.org/0000-0002-0092-1008; Email: e.c.johnson@sheffield.ac.uk

Spyridon Varlas − *Department of Chemistry, University of Sheffield, Sheffield S3 7HF, U.K.;* ⬤ orcid.org/0000-0002-4171-7572; Email: s.varlas@sheffield.ac.uk

Steven P. Armes − *Department of Chemistry, University of Sheffield, Sheffield S3 7HF, U.K.;* ⬤ orcid.org/0000-0002-8289-6351; Email: s.p.armes@sheffield.ac.uk

Authors

Oleta Norvilaite − *Department of Chemistry, University of Sheffield, Sheffield S3 7HF, U.K.*

Thomas J. Neal − *Department of Chemistry, University of Sheffield, Sheffield S3 7HF, U.K.*

Emma E. Brotherton − *Department of Chemistry, University of Sheffield, Sheffield S3 7HF, U.K.*

George Sanderson − *GEO Specialty Chemicals, Southampton SO45 3ZG, U.K.*

Graham J. Leggett − *Department of Chemistry, University of Sheffield, Sheffield S3 7HF, U.K.;* ⬤ orcid.org/0000-0002-4315-9076

Complete contact information is available at:
https://pubs.acs.org/10.1021/acs.chemmater.3c01227

Author Contributions

E.C.J. and S.V. contributed equally to this work. The manuscript was written through contributions of all authors. All authors have given approval to the final version of the manuscript.

Notes

The authors declare no competing financial interest.

■ ACKNOWLEDGMENTS

■ REFERENCES

(1) Lehn, J.-M. Dynamic Combinatorial Chemistry and Virtual Combinatorial Libraries. *Chem.— Eur. J.* **1999**, *5*, 2455−2463.

(2) Rowan, S. J.; Cantrill, S. J.; Cousins, G. R. L.; Sanders, J. K. M.; Stoddart, J. F. Dynamic Covalent Chemistry. *Angew. Chem., Int. Ed.* **2002**, *41*, 1460−1952.

(3) Corbett, P. T.; Leclaire, J.; Vial, L.; West, K. R.; Wietor, J.-L.; Sanders, J. K. M.; Otto, S. Dynamic Combinatorial Chemistry. *Chem. Rev.* **2006**, *37*, 3652−3711.

(4) Jin, Y.; Yu, C.; Denman, R. J.; Zhang, W. Recent advances in dynamic covalent chemistry. *Chem. Soc. Rev.* **2013**, *42*, 6634−6654.

(5) Chakma, P.; Konkolewicz, D. Dynamic Covalent Bonds in Polymeric Materials. *Angew. Chem., Int. Ed.* **2019**, *58*, 9682−9695.

(6) Thompson, M. C.; Busch, D. H. Reactions of Coördinated Ligands. II. Nickel(II) Complexes of Some Novel Tetradentate Ligands. *J. Am. Chem. Soc.* **1962**, *84*, 1762−1763.

(7) Nelson, S. M.; Knox, C. V.; McCann, M.; Drew, M. G. B. Metal-ion-controlled transamination in the synthesis of macrocyclic Schiff-base ligands. Part 1. Reactions of 2,6-diacetylpyridine and dicarbonyl compounds with 3,6-dioxaoctane-1,8-diamine. *J. Chem. Soc., Dalton Trans.* **1981**, 1669−1677.

(8) Goodwin, J. T.; Lynn, D. G. Template-directed synthesis: use of a reversible reaction. *J. Am. Chem. Soc.* **1992**, *114*, 9197−9198.

(9) Beyer, M. K.; Clausen-Schaumann, H. Mechanochemistry: The Mechanical Activation of Covalent Bonds. *Chem. Rev.* **2005**, *105*, 2921−2948.

(10) Davis, D. A.; Hamilton, A.; Yang, J.; Cremar, L. D.; Van Gough, D.; Potisek, S. L.; Ong, M. T.; Braun, P. V.; Martínez, T. J.; White, S. R.; Moore, J. S.; Sottos, N. R. Force-induced activation of covalent bonds in mechanoresponsive polymeric materials. *Nature* **2009**, *459*, 68−72.

(11) Furukawa, H.; Cordova, K. E.; O'Keeffe, M.; Yaghi, O. M. The Chemistry and Applications of Metal-Organic Frameworks. *Science* **2013**, *341*, 1230444.

(12) Cromwell, O. R.; Chung, J.; Guan, Z. Malleable and Self-Healing Covalent Polymer Networks through Tunable Dynamic Boronic Ester Bonds. *J. Am. Chem. Soc.* **2015**, *137*, 6492−6495.

(13) Wojtecki, R. J.; Meador, M. A.; Rowan, S. J. Using the dynamic bond to access macroscopically responsive structurally dynamic polymers. *Nat. Mater.* **2011**, *10*, 14−27.

(14) Oh, J. Y.; Rondeau-Gagné, S.; Chiu, Y.-C.; Chortos, A.; Lissel, F.; Wang, G.-J. N.; Schroeder, B. C.; Kurosawa, T.; Lopez, J.; Katsumata, T.; Xu, J.; Zhu, C.; Gu, X.; Bae, W.-G.; Kim, Y.; Jin, L.; Chung, J. W.; Tok, J. B. H.; Bao, Z. Intrinsically stretchable and healable semiconducting polymer for organic transistors. *Nature* **2016**, *539*, 411−415.

(15) Denissen, W.; Winne, J. M.; Du Prez, F. E. Vitrimers: permanent organic networks with glass-like fluidity. *Chem. Sci.* **2016**, *7*, 30−38.

(16) Bhattacharya, S.; Phatake, R. S.; Barnea, S. N.; Zerby, N.; Zhu, J.-J.; Shikler, R.; Lemcoff, N. G.; Jelinek, R. Fluorescent Self-Healing Carbon Dot/Polymer Gels. *ACS Nano* **2019**, *13*, 1433−1442.

(17) Bei, Y.; Ma, Y.; Song, F.; Kou, Z.; Hu, L.; Bo, C.; Jia, P.; Zhou, Y. Recent progress of biomass based self-healing polymers. *J. Appl. Polym. Sci.* **2022**, *139*, 51977.

(18) Gu, J.; Cheng, W.-P.; Liu, J.; Lo, S.-Y.; Smith, D.; Qu, X.; Yang, Z. pH-Triggered Reversible "Stealth" Polycationic Micelles. *Biomacromolecules* **2008**, *9*, 255−262.

(19) Xin, Y.; Yuan, J. Schiff's base as a stimuli-responsive linker in polymer chemistry. *Polym. Chem.* **2012**, *3*, 3045−3055.

(20) Whitaker, D. E.; Mahon, C. S.; Fulton, D. A. Thermoresponsive Dynamic Covalent Single-Chain Polymer Nanoparticles Reversibly Transform into a Hydrogel. *Angew. Chem., Int. Ed.* **2013**, *52*, 956−959.

(21) Bapat, A. P.; Ray, J. G.; Savin, D. A.; Hoff, E. A.; Patton, D. L.; Sumerlin, B. S. Dynamic-covalent nanostructures prepared by Diels−Alder reactions of styrene-maleic anhydride-derived copolymers obtained by one-step cascade block copolymerization. *Polym. Chem.* **2012**, *3*, 3112−3120.

(22) Yi, Y.; Xu, H.; Wang, L.; Cao, W.; Zhang, X. A New Dynamic Covalent Bond of Se−N: Towards Controlled Self-Assembly and Disassembly N: Towards Controlled Self-Assembly and Disassembly. *Chem.—Eur. J.* **2013**, *19*, 9506−9510.

(23) Bapat, A. P.; Roy, D.; Ray, J. G.; Savin, D. A.; Sumerlin, B. S. Dynamic-Covalent Macromolecular Stars with Boronic Ester Linkages. *J. Am. Chem. Soc.* **2011**, *133*, 19832−19838.

(24) Jackson, A. W.; Fulton, D. A. Making polymeric nanoparticles stimuli-responsive with dynamic covalent bonds. *Polym. Chem.* **2013**, *4*, 31−45.

(25) Cunningham, V. J.; Alswieleh, A. M.; Thompson, K. L.; Williams, M.; Leggett, G. J.; Armes, S. P.; Musa, O. M. Poly(glycerol monomethacrylate)−Poly(benzyl methacrylate) Diblock Copolymer

Nanoparticles via RAFT Emulsion Polymerization: Synthesis, Characterization, and Interfacial Activity. *Macromolecules* **2014**, *47*, 5613−5623.

(26) Deng, R.; Derry, M. J.; Mable, C. J.; Ning, Y.; Armes, S. P. Using Dynamic Covalent Chemistry To Drive Morphological Transitions: Controlled Release of Encapsulated Nanoparticles from Block Copolymer Vesicles. *J. Am. Chem. Soc.* **2017**, *139*, 7616−7623.

(27) Deng, R.; Ning, Y.; Jones, E. R.; Cunningham, V. J.; Penfold, N. J. W.; Armes, S. P. Stimulus-responsive block copolymer nano-objects and hydrogels via dynamic covalent chemistry. *Polym. Chem.* **2017**, *8*, 5374−5380.

(28) Kloxin, C. J.; Scott, T. F.; Adzima, B. J.; Bowman, C. N. Covalent Adaptable Networks (CANs): A Unique Paradigm in Cross-Linked Polymers. *Macromolecules* **2010**, *43*, 2643−2653.

(29) Kloxin, C. J.; Bowman, C. N. Covalent adaptable networks: smart, reconfigurable and responsive network systems. *Chem. Soc. Rev.* **2013**, *42*, 7161−7173.

(30) Xu, J.; Liu, Y.; Hsu, S.-h. Hydrogels Based on Schiff Base Linkages for Biomedical Applications. *Molecules* **2019**, *24*, 3005.

(31) Bilgic, T.; Klok, H.-A. Oligonucleotide Immobilization and Hybridization on Aldehyde-Functionalized Poly(2-hydroxyethyl methacrylate) Brushes. *Biomacromolecules* **2015**, *16*, 3657−3665.

(32) Brotherton, E. E.; Jesson, C. P.; Warren, N. J.; Smallridge, M. J.; Armes, S. P. New Aldehyde-Functional Methacrylic Water-Soluble Polymers. *Angew. Chem., Int. Ed.* **2021**, *60*, 12032−12037.

(33) Brotherton, E. E.; Smallridge, M. J.; Armes, S. P. Aldehyde-Functional Diblock Copolymer Nano-objects via RAFT Aqueous Dispersion Polymerization. *Biomacromolecules* **2021**, *22*, 5382−5389.

(34) Brotherton, E. E.; Neal, T. J.; Kaldybekov, D. B.; Smallridge, M. J.; Khutoryanskiy, V. V.; Armes, S. P. Aldehyde-functional thermoresponsive diblock copolymer worm gels exhibit strong mucoadhesion. *Chem. Sci.* **2022**, *13*, 6888−6898.

(35) Brotherton, E. E.; Josland, D.; György, C.; Johnson, E. C.; Chan, D. H. H.; Smallridge, M. J.; Armes, S. P. Histidine-Functionalized Diblock Copolymer Nanoparticles Exhibit Enhanced Adsorption onto Planar Stainless Steel. *Macromol. Rapid Commun.* **2023**, 2200903.

(36) Brotherton, E. E.; Johnson, E. C.; Smallridge, M. J.; Hammond, D. B.; Leggett, G. J.; Armes, S. P. Hydrophilic Aldehyde-Functional Polymer Brushes: Synthesis, Characterization, and Potential Bio-applications. *Macromolecules* **2023**, *56*, 2070−2080.

(37) Santer, S.; Rühe, J. Motion of nano-objects on polymer brushes. *Polymer* **2004**, *45*, 8279−8297.

(38) Balazs, A. C.; Emrick, T.; Russell, T. P. Nanoparticle Polymer Composites: Where Two Small Worlds Meet. *Science* **2006**, *314*, 1107−1110.

(39) Snaith, H. J.; Whiting, G. L.; Sun, B.; Greenham, N. C.; Huck, W. T. S.; Friend, R. H. Self-Organization of Nanocrystals in Polymer Brushes. Application in Heterojunction Photovoltaic Diodes. *Nano Lett.* **2005**, *5*, 1653−1657.

(40) Azzaroni, O.; Brown, A. A.; Cheng, N.; Wei, A.; Jonas, A. M.; Huck, W. T. S. Synthesis of gold nanoparticles inside polyelectrolyte brushes. *J. Mater. Chem.* **2007**, *17*, 3433−3439.

(41) Oren, R.; Liang, Z.; Barnard, J. S.; Warren, S. C.; Wiesner, U.; Huck, W. T. S. Organization of Nanoparticles in Polymer Brushes. *J. Am. Chem. Soc.* **2009**, *131*, 1670−1671.

(42) Tokareva, I.; Minko, S.; Fendler, J. H.; Hutter, E. Nanosensors Based on Responsive Polymer Brushes and Gold Nanoparticle Enhanced Transmission Surface Plasmon Resonance Spectroscopy. *J. Am. Chem. Soc.* **2004**, *126*, 15950−15951.

(43) Varlas, S.; Georgiou, P. G.; Bilalis, P.; Jones, J. R.; Hadjichristidis, N.; O'Reilly, R. K. Poly(sarcosine)-Based Nano-Objects with Multi-Protease Resistance by Aqueous Photoinitiated Polymerization-Induced Self-Assembly (Photo-PISA). *Biomacromolecules* **2018**, *19*, 4453−4462.

(44) Li, Y.; Armes, S. P. RAFT Synthesis of Sterically Stabilized Methacrylic Nanolatexes and Vesicles by Aqueous Dispersion Polymerization. *Angew. Chem., Int. Ed.* **2010**, *49*, 4042−4046.

(45) Blanazs, A.; Madsen, J.; Battaglia, G.; Ryan, A. J.; Armes, S. P. Mechanistic Insights for Block Copolymer Morphologies: How Do Worms Form Vesicles? *J. Am. Chem. Soc.* **2011**, *133*, 16581−16587.

(46) Pedersen, J. S.; Gerstenberg, M. C. Scattering Form Factor of Block Copolymer Micelles. *Macromolecules* **1996**, *29*, 1363−1365.

(47) Cornel, E. J.; van Meurs, S.; Smith, T.; O'Hora, P. S.; Armes, S. P. In Situ Spectroscopic Studies of Highly Transparent Nanoparticle Dispersions Enable Assessment of Trithiocarbonate Chain-End Fidelity during RAFT Dispersion Polymerization in Nonpolar Media. *J. Am. Chem. Soc.* **2018**, *140*, 12980−12988.

(48) Hunter, S. J.; Lovett, J. R.; Mykhaylyk, O. O.; Jones, E. R.; Armes, S. P. Synthesis of diblock copolymer spheres, worms and vesicles via RAFT aqueous emulsion polymerization of hydroxybutyl methacrylate. *Polym. Chem.* **2021**, *12*, 3629−3639.

(49) Smith, M. B.; March, J. *March's Advanced Organic Chemistry: Reactions, Mechanisms, and Structure*; John Wiley & Sons, Inc.: Hoboken, New Jersey, 2007.

(50) Johnson, E. C.; Willott, J. D.; de Vos, W. M.; Wanless, E. J.; Webber, G. B. Interplay of Composition, pH, and Temperature on the Conformation of Multi-stimulus-responsive Copolymer Brushes: Comparison of Experiment and Theory. *Langmuir* **2020**, *36*, 5765−5777.

(51) Brittain, W. J.; Minko, S. A structural definition of polymer brushes. *J. Polym. Sci., Part A: Polym. Chem.* **2007**, *45*, 3505−3512.

(52) Madsen, J.; Ducker, R. E.; Al Jaf, O.; Cartron, M. L.; Alswieleh, A. M.; Smith, C. H.; Hunter, C. N.; Armes, S. P.; Leggett, G. J. Fabrication of microstructured binary polymer brush "corrals" with integral pH sensing for studies of proton transport in model membrane systems. *Chem. Sci.* **2018**, *9*, 2238−2251.

(53) Alswieleh, A. M.; Cheng, N.; Leggett, G. J.; Armes, S. P. Spatial Control over Cross-Linking Dictates the pH-Responsive Behavior of Poly(2-(tert-butylamino)ethyl methacrylate) Brushes. *Langmuir* **2014**, *30*, 1391−1400.

(54) Cheng, N.; Bao, P.; Evans, S. D.; Leggett, G. J.; Armes, S. P. Facile Formation of Highly Mobile Supported Lipid Bilayers on Surface-Quaternized pH-Responsive Polymer Brushes. *Macromolecules* **2015**, *48*, 3095−3103.

(55) Edmondson, S.; Huck, W. T. S. Controlled growth and subsequent chemical modification of poly(glycidyl methacrylate) brushes on silicon wafers. *J. Mater. Chem.* **2004**, *14*, 730−734.

(56) Goh, S. H.; Lee, S. Y.; Dai, J.; Tan, K. L. X-ray photoelectron spectroscopic studies of ionic interactions between sulfonated polystyrene and poly(styrene-co-4-vinylpyridine). *Polymer* **1996**, *37*, 5305−5308.

(57) Abiman, P.; Wildgoose, G. G.; Crossley, A.; Jones, J. H.; Compton, R. G. Contrasting pKa of Protonated Bis(3-aminopropyl)-Terminated Polyethylene Glycol "Jeffamine" and the Associated Thermodynamic Parameters in Solution and Covalently Attached to Graphite Surfaces. *Chem.—Eur. J.* **2007**, *13*, 9663−9667.

(58) Park, J.-S.; Lim, Y.-B.; Kwon, Y.-M.; Jeong, B.; Choi, Y. H.; Kim, S. W. Liposome fusion induced by pH-sensitive copolymer: Poly(4-vinylpyridine-co-N,N′-diethylaminoethyl methacrylate). *J. Polym. Sci., Part A: Polym. Chem.* **1999**, *37*, 2305−2309.

(59) Bütün, V.; Armes, S. P.; Billingham, N. C. Synthesis and aqueous solution properties of near-monodisperse tertiary amine methacrylate homopolymers and diblock copolymers. *Polymer* **2001**, *42*, 5993−6008.

(60) Kocak, G.; Tuncer, C.; Bütün, V. pH-Responsive polymers. *Polym. Chem.* **2017**, *8*, 144−176.

(61) Willott, J. D.; Humphreys, B. A.; Webber, G. B.; Wanless, E. J.; de Vos, W. M. Combined Experimental and Theoretical Study of Weak Polyelectrolyte Brushes in Salt Mixtures. *Langmuir* **2019**, *35*, 2709−2718.

(62) Barbey, R.; Laporte, V.; Alnabulsi, S.; Klok, H.-A. Postpolymerization Modification of Poly(glycidyl methacrylate) Brushes: An XPS Depth-Profiling Study. *Macromolecules* **2013**, *46*, 6151−6158.

(63) Steinbach, A.; Paust, T.; Pluntke, M.; Marti, O.; Volkmer, D. Selective Adsorption of Functionalized Nanoparticles to Patterned

Polymer Brush Surfaces and Its Probing with an Optical Trap. *ChemPhysChem* **2013**, *14*, 3523−3531.

(64) Marschelke, C.; Puretskiy, N.; Raguzin, I.; Melnyk, I.; Ionov, L.; Synytska, A. Effect of Architecture of Thermoresponsive Copolymer Brushes on Switching of Their Adsorption Properties. *Macromol. Chem. Phys.* **2019**, *220*, 1900030.

(65) Zeuthen, C. M.; Shahrokhtash, A.; Sutherland, D. S. Nanoparticle Adsorption on Antifouling Polymer Brushes. *Langmuir* **2019**, *35*, 14879−14889.

(66) Hayes, R. A.; Böhmer, M. R.; Fokkink, L. G. J. A Study of Silica Nanoparticle Adsorption Using Optical Reflectometry and Streaming Potential Techniques. *Langmuir* **1999**, *15*, 2865−2870.

(67) György, C.; Kirkman, P. M.; Neal, T. J.; Chan, D. H. H.; Williams, M.; Smith, T.; Growney, D. J.; Armes, S. P. Enhanced Adsorption of Epoxy-Functional Nanoparticles onto Stainless Steel Significantly Reduces Friction in Tribological Studies. *Angew. Chem., Int. Ed.* **2023**, *62*, No. e202218397.

(68) Chen, Y.; Chen, J. Z. Y. Absorption and engulfing transitions in nanoparticle infiltration into a polymer brush: A monte carlo simulation. *J. Polym. Sci., Part B: Polym. Phys.* **2012**, *50*, 21−26.

(69) de Vos, W. M.; Leermakers, F. A. M.; de Keizer, A.; Kleijn, J. M.; Cohen Stuart, M. A. Interaction of Particles with a Polydisperse Brush: A Self-Consistent-Field Analysis. *Macromolecules* **2009**, *42*, 5881−5891.

(70) Halperin, A.; Kröger, M.; Zhulina, E. B. Colloid-Brush Interactions: The Effect of Solvent Quality. *Macromolecules* **2011**, *44*, 3622−3638.

(71) de Beer, S.; Mensink, L. I. S.; Kieviet, B. D. Geometry-Dependent Insertion Forces on Particles in Swollen Polymer Brushes. *Macromolecules* **2016**, *49*, 1070−1078.

(72) Laktionov, M. Y.; Shavykin, O. V.; Leermakers, F. A. M.; Zhulina, E. B.; Borisov, O. V. Colloidal particles interacting with a polymer brush: a self-consistent field theory. *Phys. Chem. Chem. Phys.* **2022**, *24*, 8463−8476.

(73) Ramakrishna, S. N.; Nalam, P. C.; Clasohm, L. Y.; Spencer, N. D. Study of Adhesion and Friction Properties on a Nanoparticle Gradient Surface: Transition from JKR to DMT Contact Mechanics. *Langmuir* **2013**, *29*, 175−182.

(74) Fernandez, N.; Cayer-Barrioz, J.; Isa, L.; Spencer, N. D. Direct, Robust Technique for the Measurement of Friction between Microspheres. *Langmuir* **2015**, *31*, 8809−8817.

(75) Morse, A. J.; Edmondson, S.; Dupin, D.; Armes, S. P.; Zhang, Z.; Leggett, G. J.; Thompson, R. L.; Lewis, A. L. Biocompatible polymer brushes grown from model quartz fibres: synthesis, characterisation and in situ determination of frictional coefficient. *Soft Matter* **2010**, *6*, 1571−1579.

(76) Al-Jaf, O.; Alswieleh, A.; Armes, S. P.; Leggett, G. J. Nanotribological properties of nanostructured poly(cysteine methacrylate) brushes. *Soft Matter* **2017**, *13*, 2075−2084.

(77) Yu, Y.; Yao, Y.; van Lin, S.; de Beer, S. Specific anion effects on the hydration and tribological properties of zwitterionic phosphorylcholine-based brushes. *Eur. Polym. J.* **2019**, *112*, 222−227.

(78) Marti, A.; Haehner, G.; Spencer, N. D. Sensitivity of Frictional Forces to pH on a Nanometer Scale: A Lateral Force Microscopy Study. *Langmuir* **1995**, *11*, 4632−4635.

(79) Carpick, R. W.; Salmeron, M. Scratching the Surface: Fundamental Investigations of Tribology with Atomic Force Microscopy. *Chem. Rev.* **1997**, *97*, 1163−1194.

(80) Tsukruk, V. V.; Bliznyuk, V. N. Adhesive and Friction Forces between Chemically Modified Silicon and Silicon Nitride Surfaces. *Langmuir* **1998**, *14*, 446−455.

(81) Berman, A.; Drummond, C.; Israelachvili, J. Amontons' law at the molecular level. *Tribol. Lett.* **1998**, *4*, 95−101.

(82) Brewer, N. J.; Beake, B. D.; Leggett, G. J. Friction Force Microscopy of Self-Assembled Monolayers: Influence of Adsorbate Alkyl Chain Length, Terminal Group Chemistry, and Scan Velocity. *Langmuir* **2001**, *17*, 1970−1974.

(83) Kim, H. I.; Graupe, M.; Oloba, O.; Koini, T.; Imaduddin, S.; Lee, T. R.; Perry, S. S. Molecularly Specific Studies of the Frictional Properties of Monolayer Films: A Systematic Comparison of CF3-(CH3)2CH-and CH3-Terminated Films. *Langmuir* **1999**, *15*, 3179−3185.

(84) Liu, W.; Simič, R.; Liu, Y.; Spencer, N. D. Effect of contact geometry on the friction of acrylamide hydrogels with different surface structures. *Friction* **2022**, *10*, 360−373.

(85) Goren, T.; Spencer, N. D.; Crockett, R. Impact of chain morphology on the lubricity of surface-grafted polysaccharides. *RSC Adv.* **2014**, *4*, 21497−21503.

(86) Singh, M. K.; Ilg, P.; Espinosa-Marzal, R. M.; Spencer, N. D.; Kröger, M. Influence of Chain Stiffness, Grafting Density and Normal Load on the Tribological and Structural Behavior of Polymer Brushes: A Nonequilibrium-Molecular-Dynamics Study. *Polymers* **2016**, *8*, 254.

(87) Centeno, R. C.; Altamirano, M. A. B.; Pérez, E.; Goicochea, A. G. The role of solvent quality, inhomogeneous polymer brush composition, grafting density and number of free chains on the viscosity, friction between surfaces, and their scaling laws. *Chem. Phys. Lett.* **2019**, *722*, 124−131.

(88) Anancharungsuk, W.; Taweepreda, W.; Wirasate, S.; Thonggoom, R.; Tangboriboonrat, P. Reduction of surface friction of natural rubber film coated with PMMA particle: Effect of particle size. *J. Appl. Polym. Sci.* **2010**, *115*, 3680−3686.

(89) Peña-Parás, L.; Gao, H.; Maldonado-Cortés, D.; Vellore, A.; García-Pineda, P.; Montemayor, O. E.; Nava, K. L.; Martini, A. Effects of substrate surface roughness and nano/micro particle additive size on friction and wear in lubricated sliding. *Tribol. Int.* **2018**, *119*, 88−98.